# Networked Nanocomposites Derived from Block Terpolymers

**Morgan Stefik, Surbhi Mahajan, Hiroaki Sai, Thomas H. Epps, III, Frank S. Bates, Sol M. Gruner, and Ulrich Wiesner**

**ABSTRACTS OF PAPERS OF THE AMERICAN CHEMICAL SOCIETY**
**August 2010, San Francisco, CA, PMSE Preprints (2010)**

# Networked Nanocomposites Derived from Block Terpolymers

**Morgan Stefik[1], Surbhi Mahajan[1,2], Hiroaki Sai[1], Thomas H. Epps, III[3,4], Frank S. Bates[3], Sol M. Gruner[5,6], and Ulrich Wiesner[1]***

*[1]Materials Science and Engineering, Cornell University, Ithaca, New York 14853.*

*[2]Present address DuPont Central Research and Development, Experimental Station, Route 141 and Henry Clay, Wilmington, DE 19880-0328.*

*[3]Department of Chemical Engineering and Materials Science, University of Minnesota, Minneapolis, Minnesota 55455.*

*[4]Present address Department of Chemical Engineering, University of Delaware, Newark, Delaware 19716.*

*[5]Department of Physics, Cornell University, Ithaca, New York 14853.*

*[6]Cornell High Energy Synchrotron Source, Cornell University, Ithaca, New York 14853.*

**Corresponding author. E-mail: ubw1@cornell.edu*

## INTRODUCTION

Nanocomposite materials will be key to next generation electrochemical devices such as batteries, supercapacitors, fuel cells, and solar cells. The ability to combine high interfacial areas, short transport distances, and volumetric access with networked pathways will facilitate devices with both higher power density and higher energy density. AB and ABA block copolymer microphase separation has been broadly applied to directing ordered nanoscale interfaces and pathways of numerous AB-type nanocomposites including mesoporous silicates[1, 2], transition metal oxides[3], and metals[4]. Such approaches rely upon specific polymer block-particle interactions to selectively swell a single block of a copolymer with nanoparticles. The coassembly of nanoparticles with block copolymers can thus result in ordered nanocomposites. Networked morphologies which have 3D cocontinuous pathways are particularly appealing for applications requiring transport. However, ordered networked nanocomposites have been quite difficult to achieve with AB-type block copolymers due in part to the very narrow 2-6 vol%[5, 6] composition window for network phases of the pure polymers.

An emerging trend in the field of structure directing with block copolymers is to expand nanostructure control to more complex architectures as well as to ABC-type nanocomposites containing three distinct domains[7-10]. A key advantage of using ABC triblock terpolymers is that they can form dozens of complex morphologies[11] including several ABC networked morphologies[12, 13]. Furthermore, we anticipate that the much wider 4-14 vol%[14, 15] composition windows for network morphologies from pure ABC polymers may facilitate the fabrication of ABC-type networked nanocomposites. Here we report the synthesis of highly ordered and networked nanocomposites from the coassembly of an ABC triblock terpolymer with oxide nanoparticles. Bottom-up coassembly approaches such as those reported here may be extended to the formation of multifunctional nanocomposites with tailored nanoarchitectures for advanced electrochemical devices.

## EXPERIMENTAL

The poly(isoprene-*b*-styrene-*b*-ethylene oxide) (ISO) triblock terpolymer used here was prepared by sequential anionic polymerization and was thoroughly characterized previously.[14] The polymer ISO4 had a number average molecular weight of 15.78 kg/mol and a polydispersity of 1.05. This polymer was composed of 44.0, 43.5, and 12.5 vol% of I, S, and O, respectively. The polymer was dissolved to ~2 wt% in a 1:1 mixture of tetrahydrofuran and chloroform. An aluminosilicate sol solution was prepared as described in detail elsewhere[1, 4] and a predetermined amount of sol was added to the polymer solution. The combined solution was stirred for an hour and cast in a covered dish on a hot plate set to 60 °C. Two samples were prepared, ISO4-S1 and ISO4-S2, which had combined O and aluminosilicate volume fractions of 23 and 30 vol%, respectively.

The films were cryomicrotomed using a Leica Ultracut UCT and stained with $OsO_4$ prior to transmission electron microscope (TEM) imaging at 120 KV on a Tecnai T12. A TEM grid containing 70 nm thick slices of ISO4-S2 was etched using a Fischione model 1020 Ar-O plasma cleaner for 10 minutes to remove the ISO polymer. Small angle x-ray scattering (SAXS) patterns were collected using a Rigaku RU300 with a copper rotating anode (λ=1.54 Å) operated at 36 kV and 50 mA. The x-rays were monochromated and focused with a Ni filter and orthogonal Franks mirrors. The 2D scattering patterns were collected with a home-built 1k x 1k pixel CCD detector similar to that described previously[16]. Data are presented as 1D plots of radially integrated intensity versus scattering vector q where $q=4\pi\sin(\theta)\lambda^{-1}$, where 2θ is the total scattering angle.

## RESULTS

Bright field TEM images of the stained nanocomposites were consistent with the core-shell double gyroid (CS-$G^D$) morphology (Fig 1A). The CS-$G^D$ is a complex network structure which contains two distinct strut networks composed of the minority end block. These strut networks are interweaving but non-intersecting and are both composed of short tubes which connect at 3-fold nodes (both struts shown in blue). Additionally, each strut network is covered with a shell of the middle block (shown in green) and resides within a matrix of the majority end block (shown in red). Both nanocomposites exhibited 3-fold and 4-fold symmetric projections which were consistent with the cubic unit cell of the CS-$G^D$. The 3-fold symmetric [111] projection of sample ISO4-S1 (Fig 1b) exhibited a wagon-wheel pattern similar to that previously reported for the CS-$G^D$ [17]. The dark, gray, and light regions correspond respectively to $O_SO_4$ stained polyisoprene, aluminosilicate containing poly(ethylene oxide), and polystyrene. The 4-fold symmetric [100] projection was also observed for sample ISO4-S1 (Fig 2c). Measurements from numerous images were taken to estimate the dimension of the unit cell $d_{100}$ to be ~63 nm on average. Similar results were observed from TEM analysis of sample ISO4-S2. Projections of 3-fold wagon-wheel patterns (Fig 1d) and 4-fold patterns (not shown) were also observed for sample ISO4-S2 consistent with the preservation of the CS-$G^D$ morphology to a higher aluminosilicate content. Measurements from TEM images of sample ISO4-S2 were used to determine an average unit cell $d_{100}$ dimension of ~53 nm. A decrease in unit cell dimension with increased aluminosilicate nanoparticle content was unexpected. However, TEM measurements from microtomed samples have significant ~15% variation due to distortion from the cutting process as well as strain induced from rearrangement of low glass transition temperature blocks such as polyisoprene. More accurate and precise measurements of the bulk $d_{100}$ spacing were obtained from SAXS experiments.

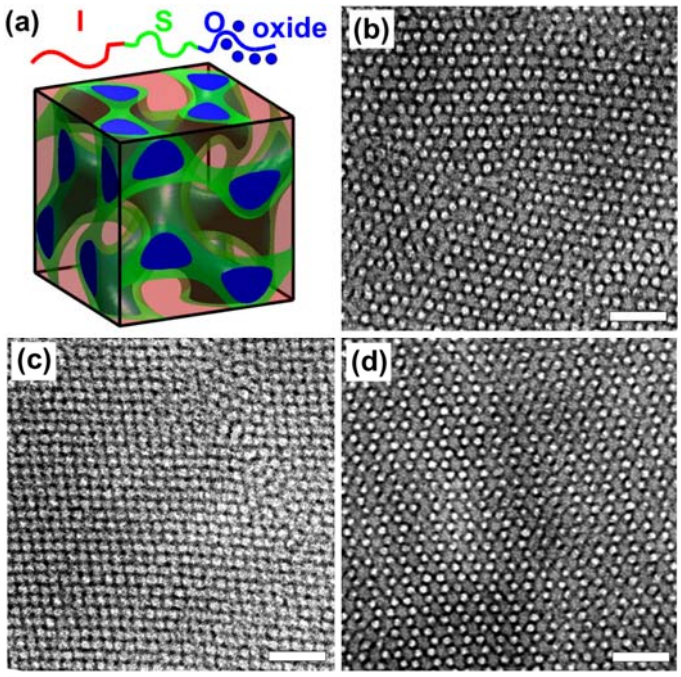


**Figure 1.** A model of the core-shell double gyroid morphology (a) is presented as a visual aid where the red, green, and blue volumes represent I, S, and O with aluminosilicate, respectively. Bright field TEM images were taken of stained samples ISO4-S1 (b,c) and ISO4-S2 (d) which were consistent with the [111] projection (b,d) and [100] projection of the core-shell double gyroid morphology. The darkest regions correspond to $OsO_4$ stained polyisoprene, the gray areas to aluminosilicate mixed with poly(ethylene oxide), and the lightest to polystyrene. All scale bars are 100 nm long.

The unit cell symmetry and size for each nanocomposite was investigated further using SAXS. The 1D integrated patterns from sample ISO4-S1 contained several higher order reflections which strengthened the structural identification. The peaks closely matched the expected sequence of $(q/q^*)^2$ = 6, 8, 14, 16, 20, 22 and 24 for the *Ia*3d space group number 230 of CS-$G^D$ morphology (Fig 2a). The $d_{100}$ spacing calculated from the most intense $(q/q^*)^2$= 6 peak was 52.9 nm which was similar to the 63 nm dimension observed by TEM. The presence of low intensity forbidden peaks at $(q/q^*)^2$ = 2, 4, 10, 12, and 18 have been predicted and observed before in silica containing films with *Ia*3d symmetry which had casting induced compression along the film normal[18-20]. The particular forbidden peaks which become allowed and their intensities likely vary with crystallographic texture as well as the silica content and evaporation conditions. The precise nature of the appearing forbidden peaks could be resolved with detailed structure factor calculations which were not attempted here. Sample ISO4-S2 had a similar SAXS pattern and indexed well to CS-$G^D$ symmetry albeit with fewer well defined higher order peaks (Fig 2b). The $d_{100}$ spacing was calculated to be 56.2 nm from the $(q/q^*)^2$= 6 peak and was similar to the 53 nm spacing observed by TEM. The 6% increase in $d_{100}$ spacing determined by SAXS corresponded to a 18% increase in unit cell volume which was consistent with the expected unit cell expansion accompanying increased content of aluminosilicate nanoparticles. The combination of TEM and SAXS characterizations for both nanocomposites were consistent with the CS-$G^D$ morphology.

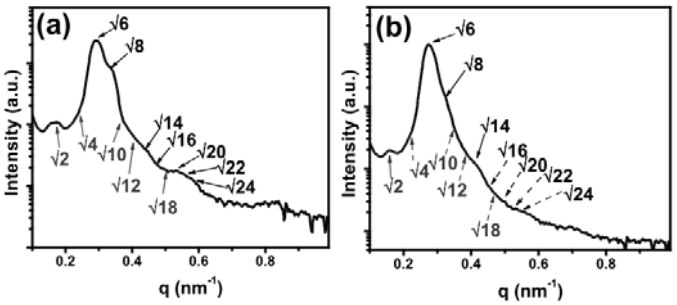


**Figure 2.** Integrated 1D small angle x-ray scattering patterns from samples ISO4-S1 (a) and ISO4-S2 (b) were consistent with the expected peaks for *Ia*3d space group symmetry of the core-shell double gyroid (indicated with black arrows). Several forbidden peaks are known to become allowed (indicated with gray arrows) in nanocomposites with evaporation induced compression.

To demonstrate the robust nature of the aluminosilicate struts the ISO polymer was removed from nanocomposite ISO4-S2 with a plasma etch. TEM images of the resulting free-standing aluminosilcate struts revealed 5 to 11 nm diameter tubes (dark) with 3-fold nodes and 29 to 37 nm mesopores suggesting preservation of the parent materials nanostructure. (Fig 3). The preservation of the aluminosilicate morphology demonstrates that the aluminosilicate particles fused together after coassembly to form a robust and continuous oxide network.

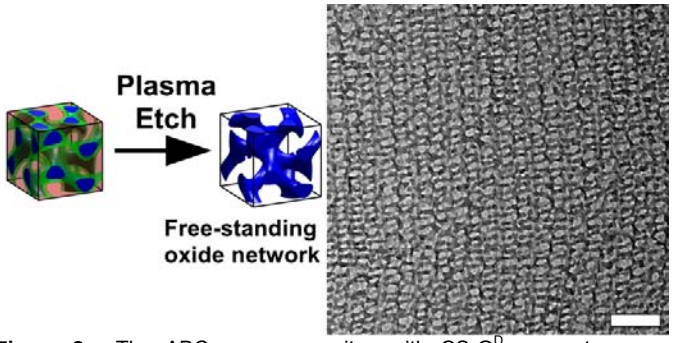


**Figure 3.** The ABC nanocomposites with CS-$G^D$ symmetry were plasma etched to remove the ISO polymer leaving behind a free-standing mesoporous aluminosilicate (left). Bright field TEM imaging of the mesoporous aluminosilicate network maintained the symmetry of parent nanocomposite ISO4-S2 (right). The scale bar is 100 nm long.

## DISCUSSION

Nanoscale control over interfaces and pathways will be key to advancing electrochemical device performance. We expect that 3D cocontinuous networked nanocomposites will be particularly well suited towards these applications. Towards this end, we demonstrated the coassembly of oxide nanoparticles with ISO polymer via a straight forward and reproducible method to synthesize ABC networked nanocomposites from the coassembly of ISO with aluminosilicate nanoparticles. The core-shell double gyroid morphology was found to form with the polymer ISO4 over a wide composition range of 23-30 vol% for the combined poly(ethylene oxide) and aluminosilicate domain. This wide 7 vol% composition window for ABC-type network formation was similar to the large composition window for network morphologies observed for pure ISO polymer.[12, 13] The stability of such oxide minority networks may be further rationalized in terms of the increased polydispersity of the combined O and aluminosilicate domain. Copolymers with blocks of different polydispersity are known to favor structures with surfaces curving towards the higher dispersity block.[21-24] Thus incorporating oxide nanoparticles into the strut containing block may increase the composition window for networked nanostructures.

The realization of 3D electrochemical devices from ISO derived nanocomposites will require transformations of the I and S domains into functional materials. One route to accomplish such multifunctional networked devices would be to remove the polymer leaving behind a free-standing oxide strut scaffold upon which functional materials may be deposited in a layer-by-layer fashion. The feasibility of the first step of this approach was demonstrated by the successful production of free-standing mesoporous aluminosilicate (Fig 3). The synthesis of layered devices in a 3D fashion may facilitate novel devices and applications. Furthermore, such mesoporous materials could be directly used for orientation independent filters.


## ACKNOWLEDGEMENTS

This work was supported by the Cornell Fuel Cell Institute via the Cornell Center for Materials Research, a Materials Research Science and Engineering Center of the National Science Foundation (NSF DMR-0520404). This publication was further supported by a Grant Number R21DE018335 from the National Institute of Dental and Craniofacial Research. This work was supported at the University of Minnesota by the NSF (DMR 0220460 and by the MRSEC Program of the National Science Foundation under Award Number DMR-0212302 and DMR-0819885). This work made use of the Cornell Center for Materials Research Shared Facilities, supported through the NSF Materials Research Science and Engineering Centers program. The X-ray equipment was supported by Department of Energy grant DEFG-02-97ER62443. CHESS was supported by the NSF and NIH-NIGMS via DMR-0225180.


## REFERENCES


1. Templin, M.; Franck, A.; DuChesne, A.; Leist, H.; Zhang, Y. M.; Ulrich, R.; Schadler, V.; Wiesner, U., *Science* **1997,** *278* (5344), 1795.
2. Zhao, D. Y.; Feng, J. L.; Huo, Q. S.; Melosh, N.; Fredrickson, G. H.; Chmelka, B. F.; Stucky, G. D., *Science* **1998,** *279* (5350), 548.
3. Yang, P. D.; Zhao, D. Y.; Margolese, D. I.; Chmelka, B. F.; Stucky, G. D., *Nature* **1998,** *396* (6707), 152.
4. Warren, S. C.; Disalvo, F. J.; Wiesner, U., *Nature Materials* **2007,** *6* (3), 248.
5. Bates, F. S.; Schulz, M. F.; Khandpur, A. K.; Forster, S.; Rosedale, J. H.; Almdal, K.; Mortensen, K., *Faraday Discuss.* **1994,** *98* (98), 7.
6. Floudas, G.; Vazaiou, B.; Schipper, F.; Ulrich, R.; Wiesner, U.; Iatrou, H.; Hadjichristidis, N., *Macromolecules* **2001,** *34* (9), 2947.
7. Toombes, G. E. S.; Mahajan, S.; Thomas, M.; Du, P.; Tate, M. W.; Gruner, S. M.; Wiesner, U., *Chem. Mater.* **2008,** *20* (10), 3278.
8. Toombes, G. E. S.; Mahajan, S.; Weyland, M.; Jain, A.; Du, P.; Kamperman, M.; Gruner, S. M.; Muller, D. A.; Wiesner, U., *Macromolecules* **2008,** *41* (3), 852.
9. Stefik, M.; Sai, H.; Sauer, K.; Gruner, S. M.; DiSalvo, F. J.; Wiesner, U., *Macromolecules* **2009,** *42* (17), 6682.
10. Stefik, M.; Mahajan, S.; Sai, H.; Epps, T. H.; Bates, F. S.; Gruner, S. M.; DiSalvo, F. J.; Wiesner, U., *Chem. Mater.* **2009**.
11. Bates, F. S., *MRS Bull.* **2005,** *30* (7), 525.
12. Epps, T. H.; Cochran, E. W.; Bailey, T. S.; Waletzko, R. S.; Hardy, C. M.; Bates, F. S., *Macromolecules* **2004,** *37* (22), 8325.
13. Chatterjee, J.; Jain, S.; Bates, F. S., *Macromolecules* **2007,** *40* (8), 2882.
14. Bailey, T. S.; Hardy, C. M.; Epps, T. H.; Bates, F. S., *Macromolecules* **2002,** *35* (18), 7007.
15. Tyler, C. A.; Qin, J.; Bates, F. S.; Morse, D. C., *Macromolecules* **2007,** *40* (13), 4654.
16. Tate, M. W.; Eikenberry, E. F.; Barna, S. L.; Wall, M. E.; Lowrance, J. L.; Gruner, S. M., *J. Appl. Crystallogr.* **1995,** *28*, 196.
17. Shefelbine, T. A.; Vigild, M. E.; Matsen, M. W.; Hajduk, D. A.; Hillmyer, M. A.; Cussler, E. L.; Bates, F. S., *J. Am. Chem. Soc.* **1999,** *121* (37), 8457.
18. Toombes, G. E. S.; Finnefrock, A. C.; Tate, M. W.; Ulrich, R.; Wiesner, U.; Gruner, S. M., *Macromolecules* **2007,** *40* (25), 8974.
19. Urade, V. N.; Wei, T.-C.; Tate, M. P.; Kowalski, J. D.; Hillhouse, H. W., *Chem. Mater.* **2007,** *19* (4), 768.
20. Crossland, E. J. W.; Kamperman, M.; Nedelcu, M.; Ducati, C.; Wiesner, U.; Smilgies, D. M.; Toombes, G. E. S.; Hillmyer, M. A.; Ludwigs, S.; Steiner, U.; Snaith, H. J., *Nano Lett.* **2009**, 2807.
21. Lynd, N. A.; Hillmyer, M. A., *Macromolecules* **2005,** *38* (21), 8803.
22. Cooke, D. M.; Shi, A. C., *Macromolecules* **2006,** *39* (19), 6661.
23. Ruzette, A. V.; Tence-Girault, S.; Leibler, L.; Chauvin, F.; Bertin, D.; Guerret, O.; Gerard, P., *Macromolecules* **2006,** *39* (17), 5804.
24. Meuler, A. J.; Ellison, C. J.; Qin, J.; Evans, C. M.; Hillmyer, M. A.; Bates, F. S., *J. Chem. Phys.* **2009,** *130* (23).